Hindawi
Advances in Materials Science and Engineering
Volume 2019, Article ID 2783784, 13 pages
https://doi.org/10.1155/2019/2783784

Research Article

Force and Deformation Characteristics during the Reconstruction and Expansion of Shallow Single-Tube Tunnels into Large-Span Multiarch Tunnels

Yanling Jia,[1,2,3] **Yongxu Xia**,[1] **Xindong Chen**,[4] **Yongdi Zhou**,[2,3] **Xingbo Han**,[1] **and Shaowen Zhou**[3]

[1]*School of Highway, Chang'an University, Xi'an, Shaanxi 710064, China*
[2]*Guangxi Key Laboratory of Road Structure and Materials, Nanning, Guangxi 530007, China*
[3]*Survey and Design Division, Guangxi Transportation Research & Consulting Co. Ltd., Nanning, Guangxi 530007, China*
[4]*School of Engineering, Cardiff University, Cardiff, Cardiff CF24 3AA, UK*

Correspondence should be addressed to Yanling Jia; 3859442@163.com and Xingbo Han; xingbo.han@chd.edu.cn

Received 2 September 2019; Accepted 10 December 2019; Published 24 December 2019

Academic Editor: Aniello Riccio

At present, there are an ever-increasing number of tunnel expansion projects in China. Studying the mechanical properties of the expanded tunnels is of great significance for guiding their safe construction. Through model testing and numerical simulation, the mechanical properties of a double-arch tunnel constructed through the expansion of the middle pilot heading from an existing single-tube tunnel were studied. The variation characteristics of the surface subsidence, surrounding rock stress, and stress and strain of the middle partition wall and lining during the tunnel reconstruction and expansion were investigated. The mechanism for transferring stress and strain between the left and right tunnel tubes was studied by a numerical simulation method. The results showed that the surface subsidence caused by the excavation of the left (i.e., the subsequent) tunnel tube was larger, and the maximum surface subsidence occurred at the right (i.e., the first) tunnel tube. The surrounding rock on the middle wall was the sensitive part of the tunnel excavation, the stress of the surrounding rock at the left spandrel of the right tunnel tube fluctuated and exhibited the most complex variation, and the stress of the surrounding rock at the right spandrel of the left tunnel tube exhibited the largest variation. The excavation of the left tunnel tube had a great influence on the forces of the middle partition wall and the lining structure of the right tunnel tube, the middle partition wall was subjected to eccentric compression towards the left tunnel tube, and the stress at the left spandrel under the initial support of the right tunnel tube exhibited complex variations. The excavation of the left and right tunnel tubes had a great influence on the stability of the surrounding rock, as well as on the force-induced deformation of the middle partition wall and the support structure, within the width of the single tunnel tube span behind the tunnel working face. Due to the different construction sequences, the stress and strain at the symmetric measurement points of the middle partition wall, as well as the left and right tunnel support structures, were very different.

1. Introduction

In recent years, the traffic volume has increased rapidly, and the road capacity built in earlier years has become increasingly insufficient. To this end, while building new roads, China has also vigorously carried out the reconstruction and expansion of the original roads. The capacity of a tunnel, as a controlling project of the road, can restrict the traffic capacity of the road. Therefore, it is particularly urgent to reconstruct and expand the original tunnels or to build new ones. Such projects have been increasingly emerging, such as the Mount Tennōzan Tunnel and Okura Tunnel in Japan and the Nazzano Tunnel in Italy, as well as the Damaoshan Tunnel of the Quanzhou Expressway, the Yuzhou Tunnel of the Chongqing Airport Road, and the expansion project of the Chongqing Eling Tunnel in China.

During the tunnel construction, the mechanical response of the structure and the surrounding rock is an important

parameter guiding the safe construction [1–4]. Researchers have extensively studied the effects of the single-tube tunnel excavation on the surface deformation and the mechanical response of the tunnel itself by using theoretical calculations [5, 6], numerical simulation [7, 8] and on-site monitoring [9, 10]. Such single-tube tunnel studies have laid the basis for the study of the mechanical response of the more complex double-tube or multiarch tunnels during excavation.

In the case of double-tube tunnels or multiarch tunnels, Addenbrooke and Potts [11] and Chehade and Shahrour [12] summarized the surface subsidence and stress characteristics of the tunnel supporting system of small-clear-distance tunnels; Hunt [13] and Divall [14] conducted extensive simulations and experiments considering various spacings and relative positions of the two tunnel tubes and analysed the variation patterns of surface subsidence; a semiempirical formula for surface subsidence prediction was proposed and modified through comparison with the formulas proposed earlier by Mair and Taylor [15] and Peck [16]. Similarly, extensively researches were carried out to predict the surface subsidence caused by the excavation of tunnels [14, 17–21]. However, none of these studies evaluated the mechanical response of the tunnel during expansion.

In general, there have been relatively few studies on the expansion of new tunnels on the basis of existing tunnels. Based on actual engineering projects, this study investigated the mechanical response of the surrounding rock and tunnel structure when a shallow single-tube tunnel is rebuilt into a double-arch tunnel. Model testing and numerical simulation were combined to obtain the force and deformation characteristics of the tunnel during reconstruction and expansion, providing a basis for subsequent construction and optimization design. The research results can also offer a reference for the implementation and theoretical research of similar projects in the future.

2. Project Overview

The original Jingya Tunnel is located on the G321 National Highway in Yangshuo County, Guilin City, Guizhou Province, China. It was built in 1993 and has a length of 120 m and a total width of 9 m. It is a second-grade road tunnel with a single tube and two-way traffic, offering the main passage into and out of the downtown area. The vegetation at the tunnel entrance and exit sections is relatively developed, the overburden layer is relatively thin, the bedrock is Devonian limestone, and the rock mass is relatively intact. The surrounding rock of the tunnel tube body is composed of slightly weathered limestone with good integrity and is classified as a Class II (with the elastic modulus between 20 and 33 GPa, the internal friction angle within 50°~60°, and the cohesion between 1.5 and 2.1 MPa) [22] surrounding rock. The existing tunnel lining is a straight wall lining cast with 30 cm thick plain concrete. With the urbanization level increase and economic development, the traffic volume has increased year by year and the daily traffic congestion has become more and more serious, and it is more difficult to travel during holidays, as shown in Figure 1.

Figure 1: Congestion at the tunnel entrance.

To meet the growing transportation needs, an in situ expansion scheme, that is, the reconstruction and expansion of an existing tunnel as a middle pilot heading into a double-arch tunnel, was determined through the comparison of different schemes based on the site topography and geological conditions, as well as comprehensively considering the requirements for the road alignment indicators and traffic planning of the reconstruction and expansion project. After the reconstruction and expansion, the width of the inner contour of the single tunnel tube is 14.803 m, the maximum excavation width is 34.146 m, and the maximum burial depth is approximately 27 m, as shown in Figure 2.

3. Model Testing Design

3.1. Determination of Similarity Ratios. The experimental similarity criteria were derived using the dimensional analysis method according to the Buckingham π theorem [23]. Considering factors such as the dimensions of the model box (2854 × 1722 × 500 mm) and the prototype span and referring to the existing research results [24, 25], the geometric similarity ratio of the model, C_l, was determined to be 60, and the similarity ratios for the other parameters can thus be obtained as follows:

$$\begin{aligned} C_\gamma &= C_\mu = C_\varepsilon = C_\varphi = 1, \\ C_\sigma &= C_E = C_c = 60, \\ C_A &= 60^2, \\ C_I &= 60^4. \end{aligned} \tag{1}$$

3.2. Similar Materials. Through the physical and mechanical property tests, similar materials for the surrounding rock, the middle partition wall, and the lining were prepared to comply with the test requirements. The mass ratio of river sand, gypsum, lime, and barite powder was 4 : 0.6 : 0.4 : 1, and additional water with a mass of 10% of that of the mixture was used to prepare the similar material for the surrounding rock, with the mechanical indicators shown in Table 1. Gypsum, water, and industrial adhesive for gypsum were mixed with a mass ratio of 1 : 0.8 : 0.5 to obtain the similar material for the middle partition wall, the initial support, and the secondary lining, with the target dimensions and physical and mechanical indicators shown in Table 2.

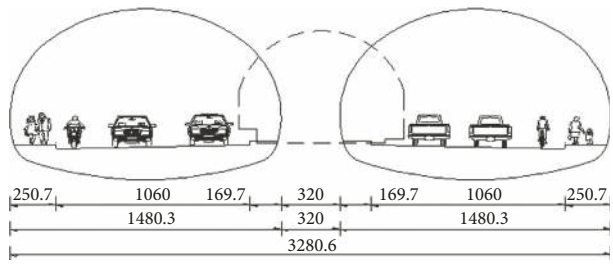

Figure 2: Cross section of the reconstructed and expanded tunnel unit (mm).

Table 1: Mechanical indicators of similar materials of the surrounding rock.

Parameter	Specific weight γ (kN/m^3)	Elastic modulus E (GPa)	Cohesion C (kPa)	Poisson's ratio μ	Internal friction angle φ (°)	Uniaxial compressive strength σ_c (MPa)
Prototype	25–27	20–33	1500–2100	0.2–0.25	50–60	57.33–76.95
Model	25–27	0.33–0.55	25–35	0.2–0.25	50–60	0.95–1.28
Material	22.28	0.524	27.16	0.19–0.22	58.38	1.104

Table 2: Thickness and mechanical parameters of the prototype and model of the lining and middle partition wall.

Parameter	Initial support thickness (mm)	Secondary lining thickness (mm)	Middle partition wall thickness (mm)	Elastic modulus E (GPa)	Compressive strength R_b (MPa)
Prototype	250 + 80.4	450	2400	23–29.5	12.5–16.7
Model	5.5	7.5	40	0.38–0.49	0.21–0.28

Note. The initial support thickness of 80.4 mm is converted to the thickness of the shotcrete with the same compressive stiffness (EA).

3.3. Arrangement of Measurement Points. The arrangement of measurement points for the displacement of the model, the internal force of the surrounding rock, and the strain of the support structure is shown in Figure 3. The dial indicator was used to monitor the change in the surface subsidence during the tunnel excavation. A total of 14 measurement points were arranged transversely along the tunnel in the middle section of the model. Limited by ground conditions, the measuring points of the in situ test were asymmetrically distributed. Thus, the measuring points of the experiment were also asymmetry distributed to keep consistent with the in situ test. Micro pressure boxes were arranged at a distance of 0 times and 0.5 times the span distance D from the initial support and the edge of the middle partition wall to monitor the change in the pressure of the surrounding rock, and 24 measurement points were arranged along the annular direction of the tunnel. The resistance strain gauges were used to monitor the strain and stress of the middle partition wall and the support structure; six measurement points were symmetrically arranged in the clockwise direction on the outer side of the middle partition wall, and eight measurement points were arranged on the inner side of the secondary lining of each of the left and right tunnel tubes, and four measurement points were arranged on the outer side of the initial support.

3.4. Experimental Excavation. The Class II surrounding rock (with the elastic modulus between 20 and 33 GPa, the internal friction angle within 50°~60°, and the cohesion between 1.5 and 2.1 MPa) [22] was simulated in the test. Therefore, the full-section excavation scheme was adopted for both the existing tunnel and the left and right tunnels, and each section was excavated only after the excavation of the previous section was completed and the corresponding monitoring data were stabilized. The excavated soil is simulated with the piece of PVC material, and different excavation footage can be simulated by taking out a different number of PVC sheets at a time. The sequence of the experimental excavation is shown in Figure 4.

4. Model Testing Result Analysis

4.1. Surface Subsidence. The test results of the surface deformation caused by the excavation of the existing tunnel, the right tunnel tube, and the left tunnel tube are plotted in Figure 5. It can be seen that, after the completion of the reconstruction and expansion, the contour of the surface subsidence is a W-shaped curve. The excavation of the subsequent (left) tunnel tube had the greatest influence on the surface deformation, followed by that of the existing tunnel, while the surface deformation caused by the excavation of the first (right) tunnel was the smallest. Such results show that the middle partition wall had a good inhibitory effect on the surface deformation caused by the first tunnel. When the subsequent tunnel tube was constructed, the surrounding rock condition was seriously deteriorated due to the multiple disturbances generated by the construction of the first tunnel tube, leading to a large increase in the surface deformation during the construction of the subsequent tunnel tube. At the same time, the maximum surface subsidence after the excavation of the left and right tunnel tubes

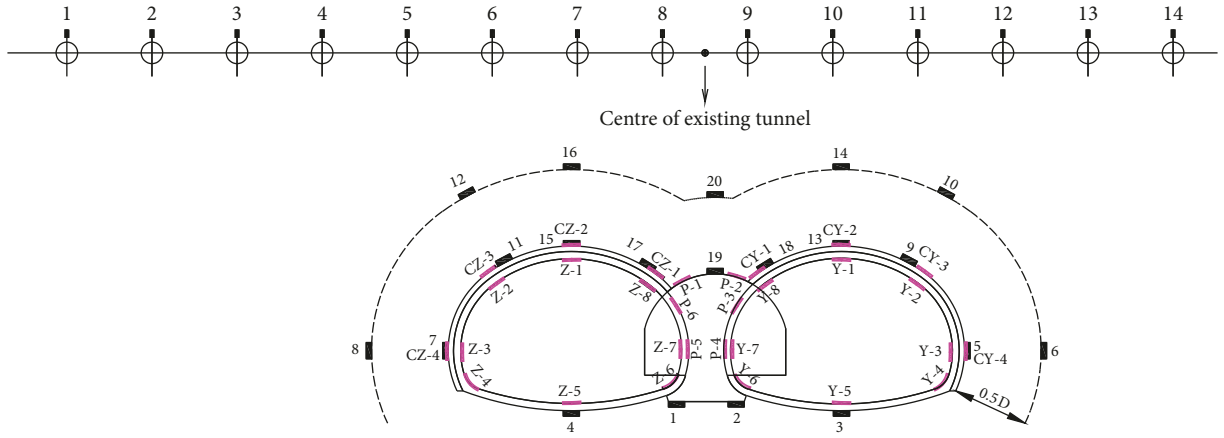

1–14 Measurement point for surface subsidence
1–20 Measurement point internal force of surrounding rock
CZ/Y 1–4 Measurement point for strain of outer side of initial support of left/right tunnel
Z/Y 1–8 Measurement point for strain of inner side of secondary lining of left/right tunnel
P 1–6 Measurement points for strain of middle partition wall

Figure 3: Arrangement of strain gauge measurement points for surrounding rock, lining, and middle partition wall.

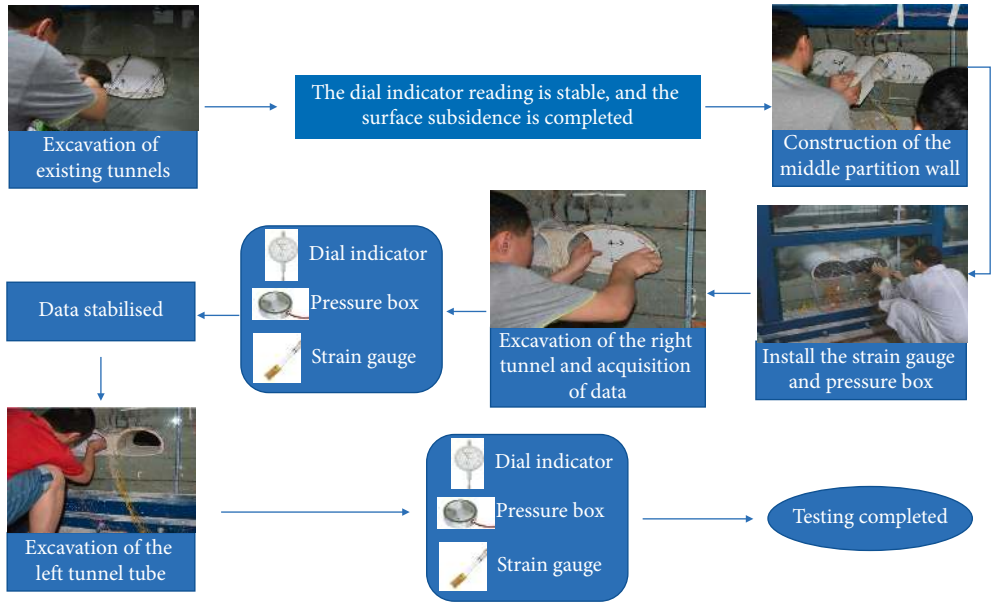

Figure 4: Schematic diagram of the excavation process for model testing.

was not directly above the surface of the centre line of the left and right tunnel tubes but slightly to the surface of the side of the middle partition wall. The maximum subsidence of the surface on the side of the right tunnel tube (0.172 mm) is larger than that on the side of the left tunnel tube (0.14 mm), indicating the lesser stability of the surrounding rock on the side of the right tunnel tube.

4.2. Surrounding Rock Stress. The original Jingya Tunnel has been completed and opened to traffic for more than 20 years, and the surrounding rock has been in a stable state. To match the conditions of the actual project, after the existing tunnel was excavated and the test data were stabilized, the middle partition wall was built, and then the pressure box data were zeroed and the data from the excavation of the right and left tunnel tubes started to be collected. To more intuitively present the results, the test data were converted to the data corresponding to the tunnel prototype according to the similarity ratios, with the negative sign indicating an increase in the pressure and the positive sign indicating a decrease in the pressure.

4.2.1. Surrounding Rock Pressure at the Bottom of the Middle Partition Wall. The time history curve of the surrounding rock pressure at the bottom of the middle partition wall is shown in Figure 6. It can be seen from the figure that, after

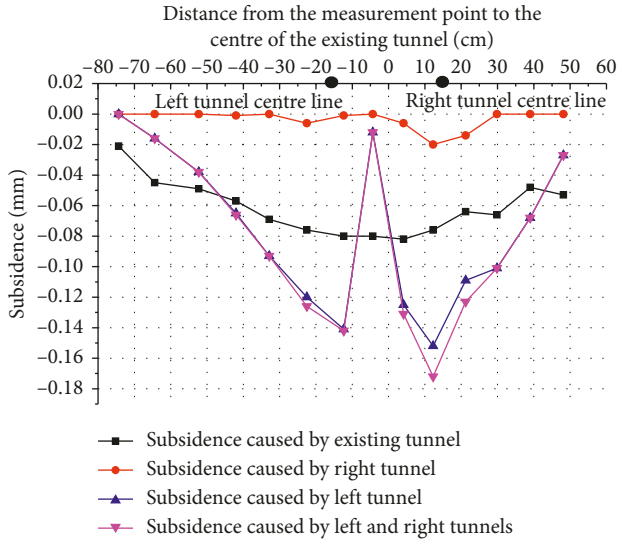

Figure 5: Surface subsidence caused by construction.

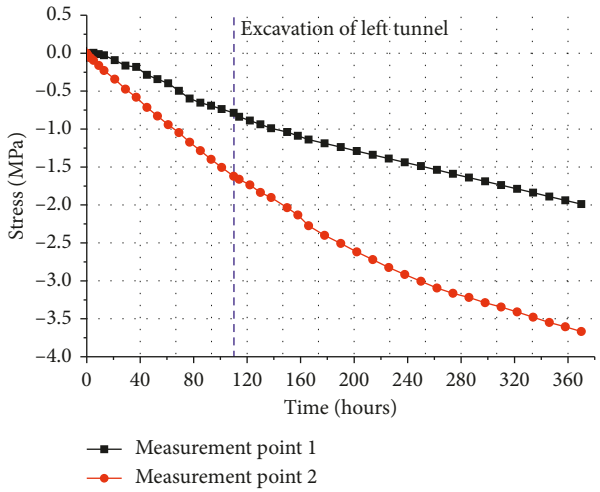

Figure 6: Time history curve of the surrounding rock stress below the toe of the middle partition wall.

the excavation of the right tunnel tube, the compressive stress of measurement points 1 and 2 at the bottom of the middle partition wall increased approximately linearly with time, and the stress increase rate of the left side (measurement point 2) was significantly larger than that of the right side (measurement point 1). The middle partition wall was subjected to eccentric compression towards the side of the left tunnel tube. When the left tunnel tube was excavated, the compressive stress at the bottom of the middle partition wall continued to increase, and the eccentric compression of the middle partition wall towards the side of the left tunnel tube was further aggravated. However, the increase rate of the pressure on the left side slowed down, and that on the right side remained basically unchanged.

4.2.2. Surrounding Rock Pressure on the Side of the Right Tunnel Tube. It can be seen from Figure 7 that, during the

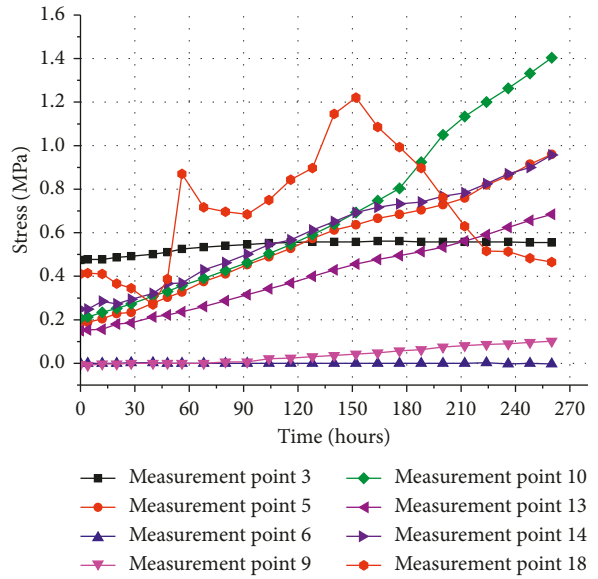

Figure 7: Time history curves of surrounding rock stresses on the right tunnel tube side.

tunnel excavation, except for at measurement point 10, which was 0.5D from the haunch, and the measurement point 6 stress at the arch spring, the surrounding rock stress at the other measurement points showed a decreasing trend. The stress variation of the surrounding rock at measurement point 18, which was 0D from the spandrel of the left arch, was more complex and first increased and then decreased, indicating the poor stability of the surrounding rock near the middle partition wall.

During the excavation of the left tunnel tube, the surrounding rock stresses at measurement points 3 and 6, which were at the bottom of the arch, did not change much; the surrounding rock stresses at measurement points 9, 13, and 14 continued to decrease, and such decrease was much larger than the stress decrease caused by the excavation of the right tunnel tube, indicating that the excavation of the left tunnel had a great influence on the stability of the surrounding rock at the vault and the spandrel of the right tunnel tube. Although the final change in the surrounding rock stress at measurement point 18 near the middle partition wall was small, the intermediate change process is the most complex, and the corresponding stress fluctuated repeatedly.

4.2.3. Surrounding Rock Pressure on the Side of the Left Tunnel Tube. It can be seen from Figure 8 that, after the excavation of the left tunnel tube, the surrounding rock stress at measurement point 4 of the bottom of the arch first decreased rapidly and then increased slowly. The surrounding rock stresses at the left haunch (measurement points 7 and 8), the left spandrel (measurement point 11), and the vault (measurement points 15 and 16) of the left tunnel tube all decreased, and such decrease was much smaller than the changes in the stresses at the corresponding measurement points of the right tunnel tube,

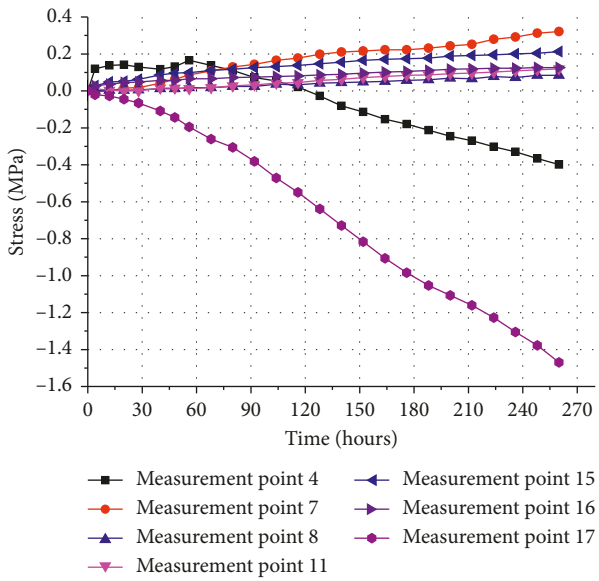

Figure 8: Time history curves of surrounding rock stresses on the left tunnel side.

indicating that the surrounding rock on the left tunnel tube side had a much better stability than that on the right tunnel tube side.

The surrounding rock stress of the right spandrel of the left tunnel tube at measurement point 17 increased by 1.47 MPa, which is much larger than the changes in the stresses at other measurement points, indicating that the surrounding rock stability was the worst at the middle partition wall. Meanwhile, in Figure 7, the surrounding rock stress at measurement point 18 corresponding to the right tunnel tube was reduced by 0.55 MPa, indicating that the surrounding rock stress on the left tunnel tube side was larger than that on the right tunnel tube side, forming eccentric compression towards the left tunnel tube side.

4.3. Middle Partition Wall and Support Structure Stresses. The test data were converted into stress data corresponding to the tunnel prototype according to the similarity ratio, where the positive sign indicates tension and the negative sign indicates compression.

4.3.1. Middle Partition Wall Stress. The stress time history curve of the middle partition wall after the expanded excavation of the tunnel is shown in Figure 9. After the excavation of the right tunnel tube, the left side of the middle partition wall (P-1) was always in tension, and the right side (P-2) is first in tension and then in compression. The left and right sides (P-6, P-3) of the spandrel of the middle partition wall were both in tension along the curved surface, and the maximum tensile stress on the left side (1.42 MPa) was 2.7 times that on the right side (0.52 MPa). The left haunch (P-5, P-4) of the middle partition wall was always in compression, and the compressive stress first increased and then decreased.

After the excavation of the left tunnel tube, the top left side (P-1) of the middle partition wall continued to be in tension, but the tensile stress gradually decreased. The top right side (P-2) was in compression, and the compressive stress gradually increased by 970%. The left and right sides of the spandrel of the middle partition wall were always in tension, and the tensile stress on the left side (P-6) decreased from 1.29 MPa to 0.86 MPa, while the tensile stress on the right side (P-3) first decreased and then increased, with a net increase of 377%. The left and right sides of the haunch of the middle partition wall were in compression, and the compressive stress gradually increased. The compressive stress on the left side (P-5) increased by 1080%, and the compressive stress on the right side (P-4) increased by 182%.

The following observations can be made. The top of the middle partition wall was, respectively, in tension and in compression along the left and right sides of the curved surface. The excavation of the left tunnel tube had a great influence on the stress of the middle partition wall; after the completion of the expansion and expansion, the left and right spandrels of the middle partition wall were in compression; the tensile stress on the right side (2.46 MPa) was 2.86 times that on the left side (0.86 MPa). The haunches on the left and right sides of the middle partition wall were both in compression, and the compressive stress on the right side (−2.34 MPa) is 1.32 times that on the left side (−1.77 MPa).

4.3.2. Initial Support Stress. After the excavation of the tunnel, the stress time history curve of the initial support of the right tunnel tube is shown in Figure 10. After the excavation of the right tunnel tube, the left spandrel (CY-1) was in tension, and the tensile stress first increased and then decreased; the stress of the vault (CY-2) was first subjected to repeated alternating tension and compression and then only compression, with the compressive stress increasing rapidly, demonstrating a complex force condition. The right spandrel (CY-3) was in compression, with the variation trend and magnitude of the compressive stress basically consistent with those of the vault. The stress at the haunch (CY-4) did not change much. After the excavation of the left tunnel tube, the stress on the left spandrel of the right tunnel tube near the side of the middle partition wall fluctuated repeatedly between tension and compression, exhibiting complex variation. The compressive stresses at the vault and the right spandrel increased significantly by 101% and 126%, respectively, and the corresponding measurement points were eventually both in compression.

After the excavation of the left tunnel tube, its initial support stress time history curve is shown in Figure 11. The following can be observed from the figure. The initial support of the left tunnel tube near the middle partition wall at the right spandrel (CZ-1) was always in compression, and the compressive stress increased with time, with the maximum value being 9.58 MPa, which was much larger than the stresses at the other three measurement points. The vault

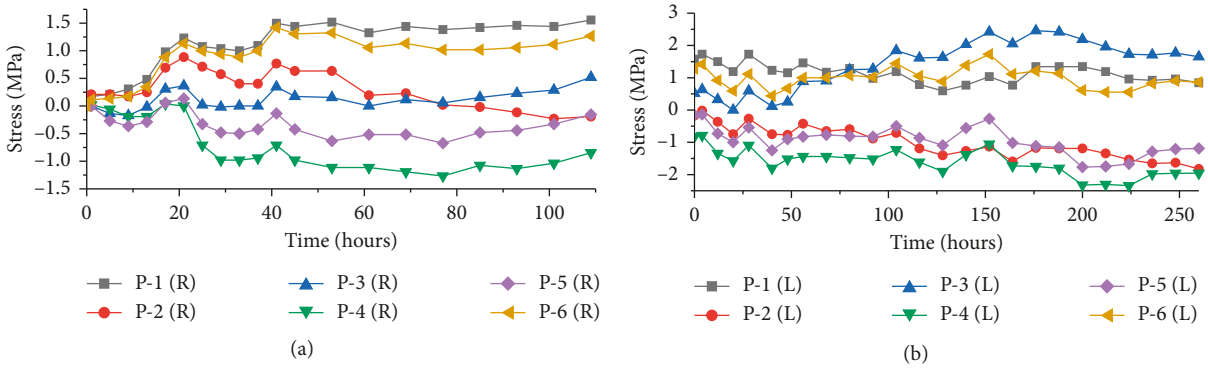

Figure 9: Stress time history curves of the middle partition wall: (a) after the excavation of the right tunnel tube; (b) after the excavation of the left tunnel tube.

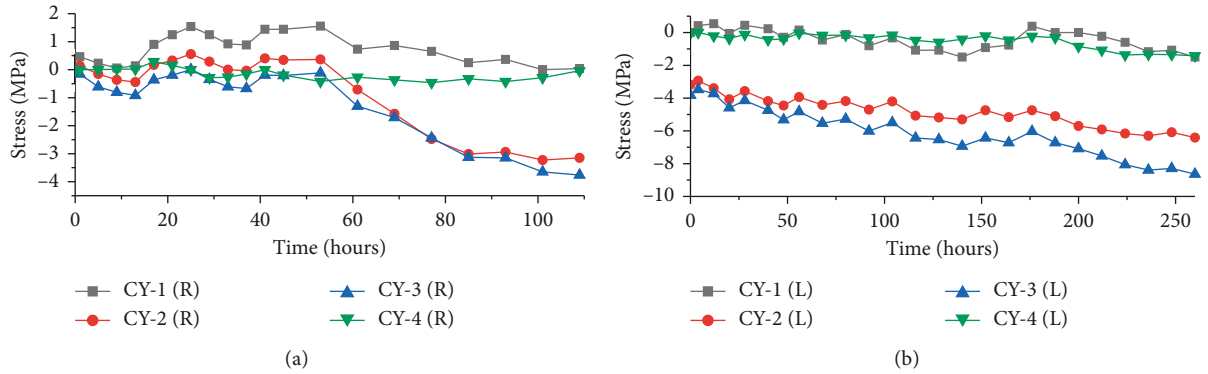

Figure 10: Time history curves of initial support stresses of the right tunnel tube: (a) after the excavation of the right tunnel tube; (b) after the excavation of the left tunnel tube.

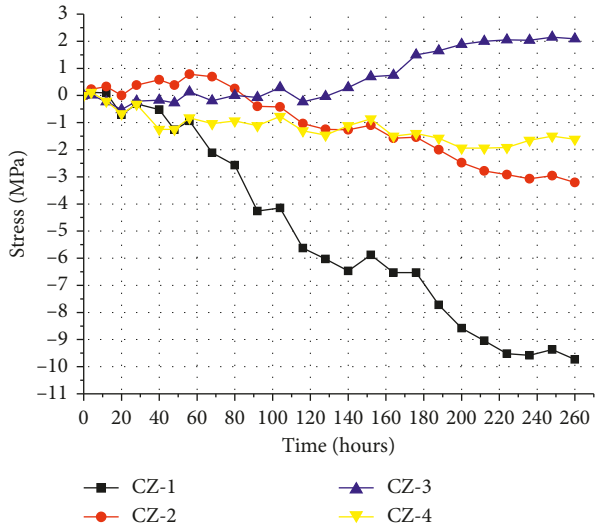

Figure 11: Time history curve of initial support stress of the left tunnel tube.

(CZ-2) was subjected to first tension and then compression. The left spandrel (CZ-3) was mainly in tension, and the left haunch (CZ-4) was in compression, with the compressive stress not changing much.

4.3.3. Secondary Lining Stress. After the excavation of the tunnel, the stress time history curve of the secondary lining of the right tunnel tube is shown in Figure 12. The arch bottom (Y-5) and the spandrels on the left and right sides (Y-8, Y-2) of the secondary lining were in tension during the excavation of the right tunnel tube and gradually changed to being in compression after the completion of the excavation. In comparison, the remaining measurement points were always in compression, with the vault (Y-1) having the largest compressive stress. The excavation of the left tunnel tube had a greater influence on the stresses at the right arch spring (Y-4), the arch bottom (Y-5), and the left haunch (Y-7) of the secondary lining of the right tunnel tube. The arch bottom and the left haunch changed from being in compression to being in tension.

Figure 13 shows the stress time history curves of the secondary lining of the left tunnel tube. It can be seen from the figure that, except for the right haunch (Z-7) of the secondary lining of the left tunnel tube being in tension, the other measurement points were all in compression. At the 230th hour, the stress at each measurement point basically stabilized. In addition, the variation of the compressive stress of the right arch spring (Z-6) near the middle partition wall size was complicated, as demonstrated by the repeated fluctuations of increases and decreases in the stress.

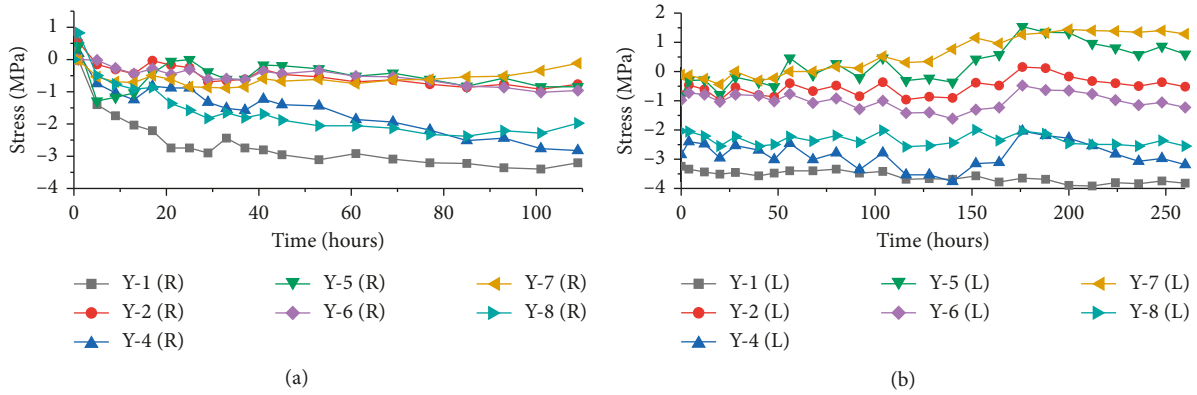

Figure 12: Stress time history curves of secondary lining of right tunnel: (a) after the excavation of the right tunnel tube; (b) after the excavation of the left tunnel tube.

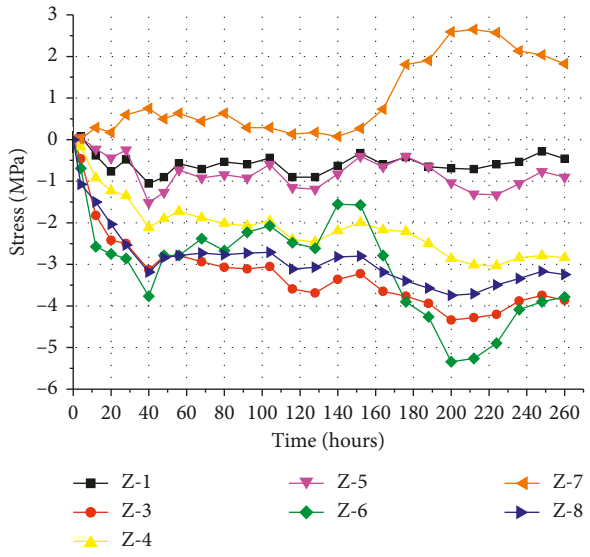

Figure 13: Time history curves of secondary lining stresses of the left tunnel tube.

A comparative analysis of Figures 9–13 shows the following. The excavation of the left tunnel had a great influence on the stress of the middle partition wall and the lining structure of the right tunnel tube, especially on the stress of the initial support of the right tunnel tube. Due to the different sequences of expansion, the variations in the stresses at the symmetric measurement points in the middle partition wall and in the support structures of the left and right tunnel tubes are very different. After the completion of the expansion and reconstruction, the tunnel structure had good stability, and the maximum stresses in the different support structures are ranked from high to low as follows: the initial support of the left tunnel tube, the initial support of the right tunnel tube, the secondary lining of the left tunnel tube, the secondary lining of the right tunnel tube, and the middle partition wall.

5. Three-Dimensional Numerical Simulation

5.1. Calculation Model and Parameters. The finite difference method numerical simulation software FLAC 3D was used to establish a three-dimensional (3D) model for the numerical simulation of the construction process. The dimensions of the three-dimensional model are $x = 188$ m, $y = 90$ m, and $z = 100$ m, and the tunnel depth is 30 m. The width of each side of the outer contour of the left and right tunnel tubes is five times the single-tunnel tube span D. The constraints of the calculation are as follows. The displacements of the left and right boundaries, as well as the bottom surface of the model, are 0, and the upper boundary is taken as a free surface. The calculation parameters of the model are shown in Table 3.

5.2. Excavation Process Simulation and Measurement Point Arrangement. To facilitate the comparison and verification of the model testing, in the numerical simulation process, first, the right tunnel is excavated, and then the left tunnel tube is excavated. The monitoring points for the middle partition wall and lining structure are shown in Figure 14.

5.3. Simulation Result Analysis

5.3.1. Surface Subsidence. The monitoring data are shown in Figure 15, where L_Y represents the distance from the working face of the right tunnel tube to the monitoring section, L_Z represents the distance from the working face of the left tunnel tube to the monitoring section, and D represents the single-tube span of the multiarch tunnel. The following can be seen from Figure 15(a). After the working face of the right tunnel tube passes through the monitoring section, the surface subsidence increases significantly as L_Y increases from $0D$ to $1D$. After the left tunnel is excavated, the surface subsidence increases greatly in the range of $-1D \le L_Z \le 1D$. As the left tunnel tube is excavated forward, the maximum surface subsidence of the monitoring section gradually shifts to the side of the left tunnel tube. In addition, when the distance of the working face from the monitoring section is larger than $1D$, the surface subsidence is less affected by the tunnel excavation.

The following can be seen from Figure 15(b). In terms of the surface subsidence caused by the separate excavation of the left and right tunnel tubes, the left tunnel tube causes a

Table 3: Parameters of the surrounding rock and support structure.

Material	Specific weight (kN/m^3)	Elastic modulus (GPa)	Poisson's ratio	Internal friction angle (°)	Cohesion (MPa)	Thickness (m)
Surrounding rock	27	20	0.25	50	1.5	—
Initial support of the original tunnel	23	23	0.2	—	—	0.45
Middle partition wall	23	31	0.2	—	—	2.4
Initial support	23	23	0.2	—	—	0.15
Secondary lining	23	29.5	0.2	—	—	0.4

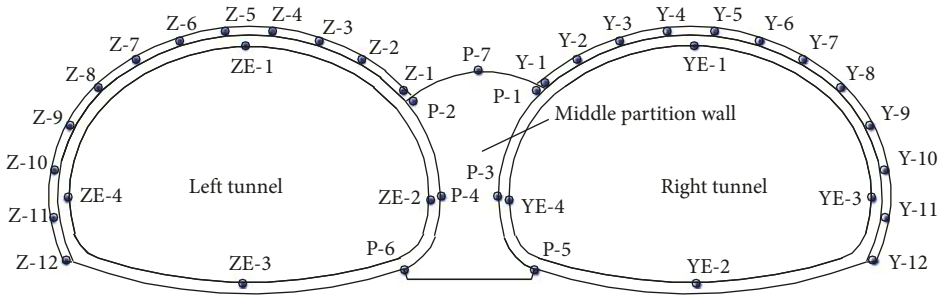

Figure 14: Arrangement of model monitoring points.

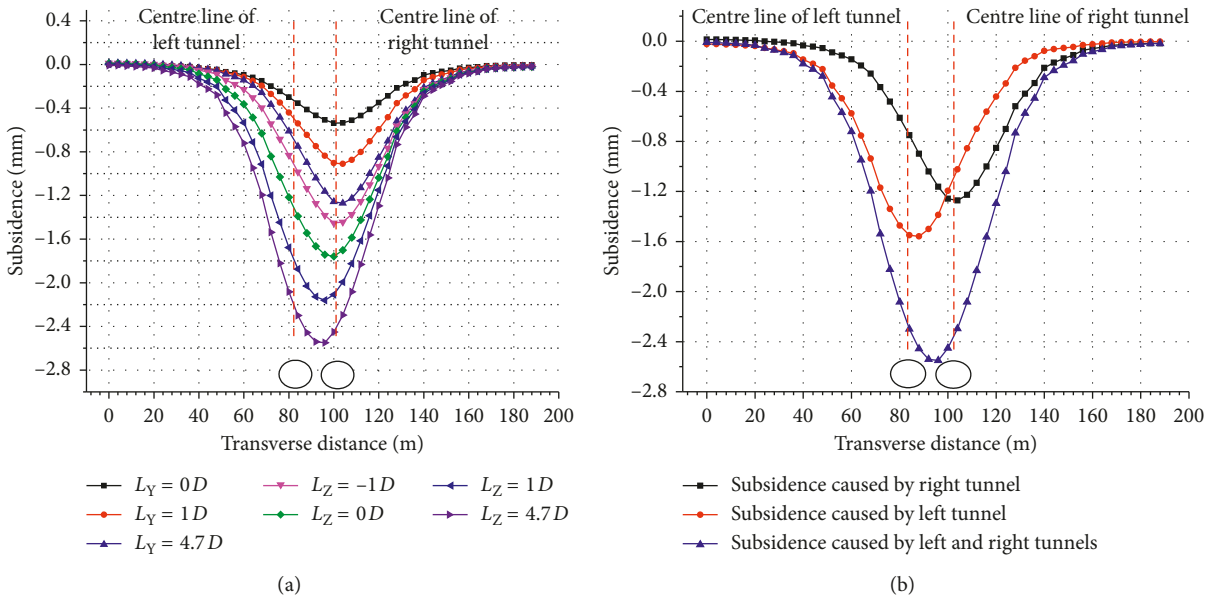

Figure 15: Monitoring data: (a) surface subsidence process; (b) surface subsidence caused by left and right tunnel tubes.

larger surface subsidence than the right tunnel tube. The maximum surface subsidence caused by the excavation of the right tunnel tube is directly above its centre line, and the maximum surface subsidence caused by the excavation of the left tunnel tube shifts to the side of the right tunnel tube. The maximum surface subsidence caused by the excavation of the left and right tunnel tubes is 2.6 mm and shifts to the right tunnel tube side.

5.3.2. Displacement at Monitoring Points of Secondary Lining. It can be clearly seen from Figure 16 that the vault sinking and the inverted arch bulging of the left and right tunnel tubes converge more significantly than the displacements of the surrounding. When the distance of the working face to the monitoring section is larger than 1D, the tunnel excavation basically no longer causes the vault to sink and the inverted arch to bulge. It can be seen from Figure 16(b) that, due to the presence of the existing tunnel on the left side, after the right tunnel tube is excavated, the left haunch of the secondary lining is deformed significantly towards the left side; after the left tunnel tube is excavated, the left haunch is deformed towards the left side.

It can be seen from Table 4 that the excavation of the left tunnel tube has a great influence on the vault sinking of the right tunnel tube and the convergence of the surrounding.

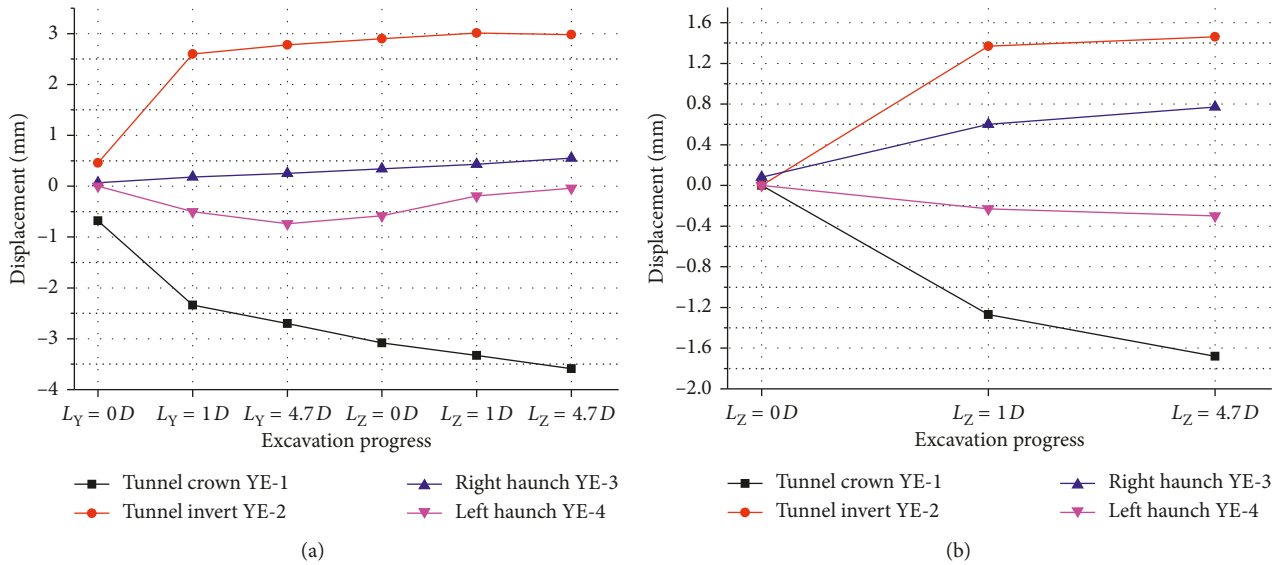

Figure 16: Displacement at monitoring points of secondary lining: (a) right tunnel; (b) left tunnel.

Table 4: Displacements of the secondary lining (mm).

Measurement point	$E_{YY}(A)$	$E_{YZ}(B)$	$E_{ZZ}(C)$	B/A(%)	C/B (%)
EY/Z-1	−2.70	−3.59	−1.68	132.81	46.73
EY/Z-2	2.78	2.98	1.46	107.28	48.89
EY/Z-3	0.25	0.55	0.77	217.33	—
EY/Z-4	−0.74	−0.04	−0.30	5.11	—

Note. E_{YY} is the displacement of measurement points of secondary lining of the right tunnel tube after the completion of the right tunnel tube excavation. E_{YZ} is the displacement of measurement points of secondary lining of the right tunnel tube after the completion of the left tunnel tube excavation. E_{ZZ} is the displacement of measurement points of secondary lining of the left tunnel tube after the completion of the left tunnel tube excavation.

The vault sinking and the inverted arch bulging of the right tunnel tube are twice those of the left tunnel tube.

5.3.3. Middle Partition Wall Stress. The following can be seen from Figure 17. When the distance from the working faces of the left and right tunnel tubes to the monitoring section is greater than 1D, the force on the middle partition wall changes little. After the excavation of the left and right tunnel tubes, the maximum stress of the middle partition wall (3.42 MPa) is at the lower portion of the left haunch.

The following can be seen from Table 5. After the excavation of the right tunnel tube, the compressive stress of the right haunch of the middle partition wall is the largest, and the compressive stresses of the corresponding measurement points on the right side (P-1, P-3, and P-5) are larger than those on the left side (P-2, P-4, and P-6). The excavation of the left tunnel tube has a significant effect on the forces of the middle partition wall. The compressive stresses at the top left (P-2), haunch (P-4), and bottom (P-6) of the middle partition wall increase to 361.64%, 397.30%, and 189.34% of the original stresses, respectively, and are greater than the

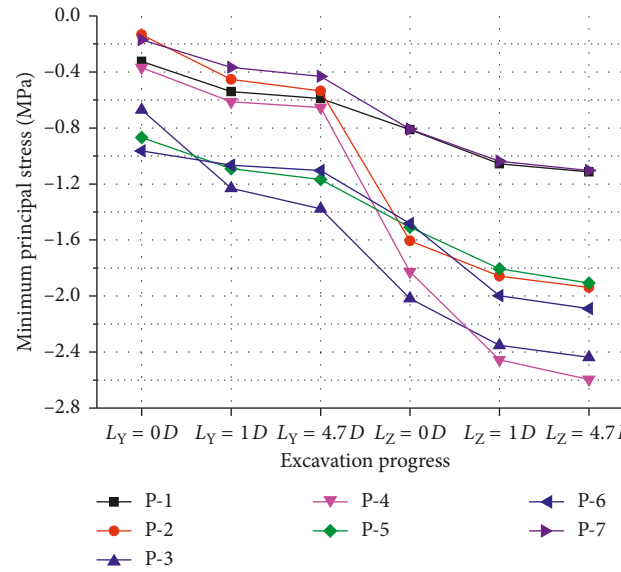

Figure 17: Variation of stresses in middle partition wall.

compressive stress of the counterpart measurement points on the right side. The forces on the middle partition wall shift towards the side of the left tunnel tube.

5.3.4. Axial Forces of the Initial Support. The following can be seen from Figure 18. When the working faces of the left and right tunnel tubes are each excavated forward by 1D ($L_Y = 1D$, $L_Z = 1D$) after passing through the monitoring section, the axial force at the haunch of the initial support of the left and right tunnel tubes increases sharply; the axial forces of the other parts also increase. As the tunnel tube continues to be excavated forward, the axial force of the initial support increases slightly. The excavation of the left and right tunnel tubes has a small influence on the axial force

Table 5: Compressive stresses at measurement points of the middle partition wall (MPa).

Measurement point	$P_Y(A)$	$P_Z(B)$	B/A(%)
P-1	−0.59043	−1.11401	188.68
P-2	−0.53609	−1.93816	361.54
P-3	−1.37772	−2.43763	176.93
P-4	−0.65321	−2.59516	397.30
P-5	−1.16796	−1.90799	163.36
P-6	−1.10355	−2.08942	189.34
P-7	−0.43117	−1.10307	255.83

Note. P_Y is the first principal stress at measurement point of the middle partition wall after completion of the right tunnel tube excavation. P_Z is the first principal stress at measurement point of the middle partition wall after completion of the left tunnel tube excavation.

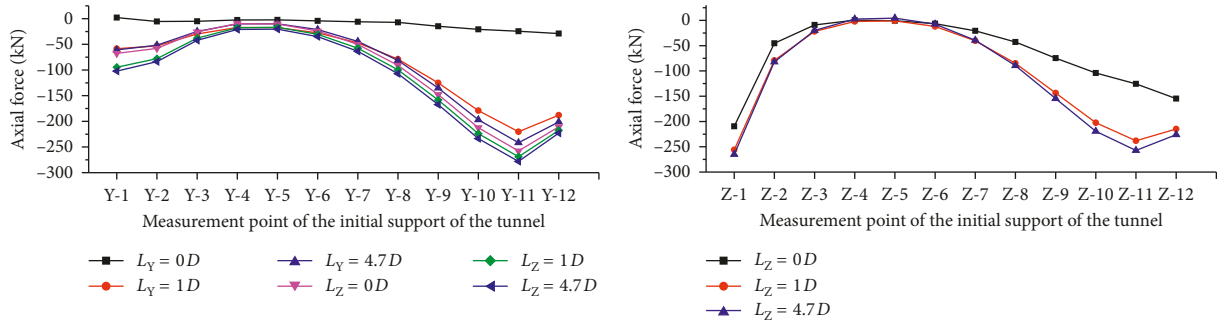

Figure 18: Axial force of initial support of tunnel: (a) right tunnel; (b) left tunnel.

at the vault of the initial support. All measurement points on the initial support of the right tunnel tube are subjected to compression. As the working face of the left tunnel tube is advanced forward, the axial force of the vault gradually changes from compression to tension.

Combined with the analysis of Table 6, it can be seen that the axial force at the haunch of the right tunnel tube is the largest, and the excavation of the left tunnel tube has a great influence on the axial force at the left spandrel of the initial support of the right tunnel tube. The axial force at the right spandrel of the left tunnel tube (−265.2 kN) is the largest, significantly larger than that at the left spandrel of the right tunnel tube (−102.1 kN). After the reconstruction and expansion, the axial forces at the corresponding measurement points of the initial supports of the left and right tunnel tubes are very different.

5.4. Comparative Analysis. A comparative analysis of the model testing and numerical simulation results was carried out, and they were found to be consistent. The following can be seen. The surface subsidence caused by the excavation of the left tunnel tube is larger than that of the right tunnel tube. After the reconstruction and expansion, the maximum surface subsidence is near the right tunnel tube side. The excavation of the left tunnel tube has a great influence on the forces on the middle partition wall, and the middle partition wall is subjected to eccentric forces towards the left tunnel tube side. The excavation of the left tunnel tube has a great influence on the stress and deformation of the initial support and the secondary lining of the right tunnel tube; the stress at the right side spandrel of the initial support of the left tunnel tube is the largest. The strain and stress of the symmetric measurement points in the middle partition wall and in the support structures of left and right tunnel tube are quite different. However, the double-arch tunnel has an overall good stability.

Table 6: Axial forces of initial supports of left and right tunnel tubes (kN).

Measurement point	$F_{YY}(A)$	$F_{YZ}(B)$	$F_{ZZ}(C)$	B/A(%)
Y/Z-1	−60.82	−102.10	−265.20	167.87
Y/Z-2	−51.66	−83.72	−82.26	162.05
Y/Z-3	−24.89	−42.12	−19.86	169.24
Y/Z-4	−10.07	−20.96	2.54	208.20
Y/Z-5	−9.87	−20.43	4.36	206.94
Y/Z-6	−21.15	−34.94	−7.53	165.18
Y/Z-7	−44.24	−63.46	−39.30	143.45
Y/Z-8	−81.42	−107.24	−89.41	131.71
Y/Z-9	−135.25	−167.34	−154.65	123.72
Y/Z-10	−196.93	−233.58	−219.30	118.61
Y/Z-11	−241.62	−277.99	−257.21	115.06
Y/Z-12	-201.11	−222.86	−226.12	110.82

Note. F_{YY} is the axial force of initial support of right tunnel tube after completion of right tunnel tube excavation. F_{YZ} is the axial force of initial support of right tunnel tube after completion of left tunnel tube excavation. F_{ZZ} is the axial force of initial support of left tunnel tube after completion of left tunnel tube excavation.

6. Conclusions

(1) Surface subsidence: the surface subsidence caused by the excavation of the left tunnel tube is larger than

that of the right tunnel tube. The maximum surface subsidence value after reconstruction and expansion is near the right tunnel tube side. Therefore, when excavating the left tunnel tube, attention should be paid to closely monitoring the surface subsidence and strictly controlling the blasting.

(2) Stress variation of surrounding rock: due to the influence of multiple excavation disturbances, the stability of the surrounding rock on both sides of the middle partition wall becomes the worst, and the stress variation of the surrounding rock of the left and right tunnel tubes near the middle partition wall is more complex. Therefore, the surrounding rock of the upper portion of the middle partition wall should be reinforced during the construction process.

(3) Stress and strain of the middle partition wall and lining structure: the excavation of the left tunnel tube has a great influence on the stress and deformation of the middle partition wall and the lining structure of the right tunnel tube. The middle partition wall is subjected to eccentric forces towards the left tunnel tube side, and the compressive stress on the right side spandrel of the initial support of the left tunnel tube is the largest. Therefore, during the construction process, attention should be paid to monitoring the force and displacement of the middle partition wall and strengthening the bottom of the middle partition wall; the force of the right side spandrel of the initial support of the left tunnel tube should be especially monitored.

(4) The excavation of the left and right tunnel tubes has a significant influence on the stability of the surrounding rock, as well as the force and deformation of the middle partition wall and the support structure within 1D behind the working face. The strain and stress at the symmetric measurement points of the middle partition wall, as well as the support structures of the left and right tunnel tubes, are very different, whereas the double-arch tunnel has an overall good stability.

(5) The characteristics of surface subsidence, as well as the stress and strain of the middle partition wall and lining during the reconstruction and expansion process as obtained by model testing and numerical simulation, are close. The two study methods have been mutually confirmed, and the obtained research results have effectively guided the reconstruction and expansion of the tunnels and provided a technical support for the smooth construction of the project. The project has been completed and opened to traffic, and the research results can provide a useful reference for similar projects in the future.

Data Availability

The data used to support the findings of this study are included within the article.

Conflicts of Interest

The authors declare that they have no conflicts of interest.

Acknowledgments

The research work reported herein was made possible by the Guangxi Scientific Research and Technology Development Plan Project (no. Guikegong 1355008-3) and Guangxi Transportation Science and Technology Project and Standardization Project (no. Guijiaokejiaofa (2014) 48). The financial support is highly appreciated.

References

[1] A. R. Beyabanaki and V. Gall, "3D numerical parametric study of the influence of open-pit mining sequence on existing tunnels," *International Journal of Mining Science and Technology*, vol. 27, no. 3, pp. 459–466, 2017.

[2] X. Han and Y. Xia, "Analytic solutions of the forces and displacements for multicentre circular arc tunnels," *Mathematical Problems in Engineering*, vol. 2018, Article ID 8409129, 14 pages, 2018.

[3] A.-Z. Lu, L.-Q. Zhang, and N. Zhang, "Analytic stress solutions for a circular pressure tunnel at pressure and great depth including support delay," *International Journal of Rock Mechanics and Mining Sciences*, vol. 48, no. 3, pp. 514–519, 2011.

[4] X. Han, Y. Xia, X. Wang, and L. Chai, "Complex variable solutions for forces and displacements of circular lined tunnels," *Mathematical Problems in Engineering*, vol. 2018, Article ID 2037845, 12 pages, 2018.

[5] X. Han, Y. Xia, F. Ye, and Y. Wang, "Ageing models and maintenance strategy for road tunnels," *Structure and Infrastructure Engineering*, pp. 1–16, 2019.

[6] X. M. Zhang, X. Ou, J. Yang, and J. Fu, "Deformation response of an existing tunnel to upper excavation of foundation pit and associated dewatering," *International Journal of Geomechanics*, vol. 17, no. 4, Article ID 04016112, 2017.

[7] M.-G. Li, J.-J. Chen, J.-H. Wang, and Y.-F. Zhu, "Comparative study of construction methods for deep excavations above shield tunnels," *Tunnelling and Underground Space Technology*, vol. 71, pp. 329–339, 2018.

[8] S. Wang, T. Qu, Y. Fang, J. Fu, and J. Yang, "Stress responses associated with earth pressure balance shield tunneling in dry granular ground using the discrete-element method," *International Journal of Geomechanics*, vol. 19, no. 7, Article ID 04019060, 2019.

[9] G. B. Liu, P. Huang, J. W. Shi, and C. W. W. Ng, "Performance of a deep excavation and its effect on adjacent tunnels in shanghai soft clay," *Journal of Performance of Constructed Facilities*, vol. 30, no. 6, Article ID 04016041, 2016.

[10] S. Wang, P. Liu, T. Qu, J. Fu, and J. Zhou, "Performance of supporting structures of a single-floor three-span metro station during column-drift tunneling in dry sandy ground," *Journal of Performance of Constructed Facilities*, vol. 32, no. 3, 2018.

[11] T. I. Addenbrooke and D. M. Potts, "Twin tunnel interaction: surface and subsurface effects," *International Journal of Geomechanics*, vol. 1, no. 2, pp. 249–271, 2001.

[12] F. H. Chehade and I. Shahrour, "Numerical analysis of the interaction between twin-tunnels: influence of the relative position and construction procedure," *Tunnelling and Underground Space Technology*, vol. 23, no. 2, pp. 210–214, 2008.

[13] D. V. Hunt, "Predicting the settlements above twin tunnels constructed in soft ground," in *Proceedings of the Tunnelling & Underground Space Technology Underground Space for Sustainable Urban Development Ita-Aites World Tunnel Congress*, Singapore, May 2004.

[14] S. Divall, *Ground Movements Associated with Twin-Tunnel Construction in Clay*, City University, London, UK, 2013.

[15] R. J. Mair and R. N. Taylor, "Theme lecture: bored tunnelling in the urban environment," in *Proceedings of the Fourteenth International Conference on Soil Mechanics and Foundation Engineering Post Conference Proceedings*, vol. 4, pp. 2353–2385, Publications Comm Of Xiv Icsmfe; Publications Comm Of Xiv, Rotterdam, Netherlands, 1999.

[16] R. B. Peck, "Deep excavations and tunnelling in soft ground: state-of-the-art report," in *Proceedings of the 7th International Conference on Soil Mechanics and Foundation Engineering*, Mexico City, 1969.

[17] D. N. Chapman, S. K. Ahn, D. V. L. Hunt, and A. H. C. Chan, "The use of model tests to investigate the ground displacements associated with multiple tunnel construction in soil," *Tunnelling and Underground Space Technology*, vol. 21, no. 3-4, p. 413, 2006.

[18] B.-L. Chu, S.-C. Hsu, Y.-L. Chang, and Y.-S. Lin, "Mechanical behavior of a twin-tunnel in multi-layered formations," *Tunnelling and Underground Space Technology*, vol. 22, no. 3, pp. 351–362, 2007.

[19] P. Li, S.-J. Du, X.-F. Ma, Z.-Y. Yin, and S.-L. Shen, "Centrifuge investigation into the effect of new shield tunnelling on an existing underlying large-diameter tunnel," *Tunnelling and Underground Space Technology*, vol. 42, no. 5, pp. 59–66, 2014.

[20] N.-A. Do, D. Dias, and P. Oreste, "Three-dimensional numerical simulation of mechanized twin stacked tunnels in soft ground," *Journal of Zhejiang University Science A*, vol. 15, no. 11, pp. 896–913, 2014.

[21] C. W. Ng, K. M. Lee, and D. K. Tang, "Three-dimensional numerical investigations of new Austrian tunnelling method (NATM) twin tunnel interactions," *Canadian Geotechnical Journal*, vol. 41, no. 3, pp. 523–539, 2004.

[22] Ministry of Transport of the People' Republic of China, *Code for Design of Road Tunnel*, China Communications Press, Beijing, China, 2014.

[23] D.-y. Li, B.-m. Wang, and Y.-C. Li, *Construction Model Experiment*, Science Press, Beijing, China, 1996.

[24] F. Gao and D.-l. Xue, "Double-arch tunnel construction in large span bias weak surrounding rock," *Journal of Chongqing Jiaotong University(Natural Science)*, vol. 14, no. 33, pp. 30–34, 2014.

[25] G. Zhao, *Study on the Modeling Tests of Double-Arch Highway Tunnel*, Southwest jiaotong University, Chengdu, China, 2005.